Electronic Supplementary Material (ESI) for Journal of Materials Chemistry A.

Electronic Supplementary Information for

Multi-bioinspired Self-cleaning Energy-free Cooling Coatings

Bing-Ying Liu[a], Chao-Hua Xue*[a,c], Hong-Mei Zhong[b], Xiao-Jing Guo[e], Hui-Di Wang[e], Hui-Gui Li[c], Mi-Mi Du[c], Meng-Chen Huang[c], Ren-Xuan Wei[c], Long-Gang Song[d], Bo Chang[d] and Zuankai Wang[b]*

a College of Environmental Science and Engineering, Shaanxi University of Science and Technology, Xi'an, China

b Department of Mechanical Engineering, City University of Hong Kong, Hong Kong, China

c College of Bioresources Chemical and Materials Engineering, Shaanxi University of Science and Technology, Xi'an, China

d College of Mechanical and Electrical Engineering, Shaanxi University of Science and Technology, Xi'an, China

e College of Materials Science and Engineering, Shaanxi University of Science and Technology, Xi'an, China

Correspondence to: xuech@sust.edu.cn (C. H.X.); zuanwang@cityu.edu.hk (Z.W.)

This PDF file includes:

Section 1. Methods

Section 1.1 Materials

Poly(vinylidene fluoride-co-hexafluoropropylene) P(VDF-HFP), average M_w ~ 400000, average M_n ~ 130000, pellets) was purchased from Sigma-Aldrich). Polydimethylsiloxane (PDMS, Sylgard 184 Silicone Elastomer Kit with components of PDMS elastomer precursor base A and curing agent B) was purchased from Dow Corning. Acetone (analytical grade, water content < 0.03 wt%) and tetrahydrofuran (THF) were obtained from Tianjin Fuyu Fine Chemical Company. Hydrochloric acid (HCl), distilled water, and sodium hydroxide (NaOH) were commercially obtained. All the chemicals were used without any further purification. Aluminum plates were purchased from a local market.

Section 1.2 Fabrication

The porous P(VDF-HFP)/PDMS film, or SRCP film, was fabricated using a facile water-induced phase-separation process. Briefly, 3.5 g of P(VDF-HFP) was dissolved in 42.0 g of acetone under stirring at the room temperature for 3 hours until P(VDF-HFP) was completely dissolved. Then 1.0 g of precursor base A for PDMS and 30.0 g of THF were added into the P(VDF-HFP) solution under stirring and 0.1 g of curing agent B was added, followed by stirring for 30 min to obtain a transparent solution. Afterward, 5.0 g of water was added dropwise to the transparent solution at a rate of 0.05 mL per 10 s under stirring to form a sol. The obtained sol was poured into a Petri dish of 90-180 mm and dried at room temperature for 3 h until the solvents and water were completely evaporated to obtain a free-standing film. The fabrication process was shown in Fig. 1. Films with thicknesses of 79, 130, 283, 380, 410, and 580 μm were produced by changing the cast amount of sol solution. To obtain the film with a thickness less than 10 μm, the sol solution was spin-coated on a glass substrate.

As a comparison, we also fabricated flat P(VDF-HFP) flim. Briefly, 3.5 g of P(VDF-HFP) was dissolved in 42.0 g of the acetone solution under stirring at room temperature for 3 h until P(VDF-HFP) was completely dissolved. The obtained solution was poured into a Petri dish of 90 mm and dried at room temperature for 2 hours until the solvent were completely evaporated, then an optically transparent flat P(VDF-HFP) film was obtained.

To fabricate the porous P(VDF-HFP) flim, 3.5 g of P(VDF-HFP) was dissolved in 42.0 g of the acetone solution under stirring at room temperature for 3 h until P(VDF-HFP) was completely dissolved. 4.0 g of water was added dropwise to the translucent solution at a rate of 0.05 ml per 10 s under stirring to form a sol. After pouring the as-obtained sol into a Petri dish of 90 mm and drying at room temperature for 3 hours, a porous P(VDF-HFP) film was obtained.

Section 1.3 Characterization

Scanning electron microscopy (SEM) images were obtained with a Hitachi S-4800 field emission scanning electron microscope operated at an acceleration voltage of 5 kV. All samples were sputter-coated with gold prior to examination. Energy-dispersive spectroscopy (EDS) was used to check elements distribution. Elemental analysis of the film surface was conducted by using a K-alpha Thermo Fisher Scientific X-ray photoelectron spectroscope (XPS) with an Al Kα radiation at a 90° take-off angle. Reflectivity in the UV-Visible and near-infrared (UV-VIS-NIR) range of 200-2500 nm was measured with a Cary 5000 UV-VIS-NIR spectrophotometer in conjunction with a 110 mm integrating sphere (Agilent Technologies). Reflectivity in the thermal-infrared range of 2500-25000 nm was measured by a Fourier Transform Infrared (FTIR) spectrometer (Bruker Tensor 27) with a gold integrating sphere. The incident angle of light to the surface was fixed for both reflectance measurements. Digital pictures were taken by a common digital camera.

Section 1.4 Measurements

Section 1.4.1 Indoor thermal measurements

Xenon lamp (Zhongjiao Jinyuan HXF300) with a high power that matches well with the solar spectrum was used to simulate solar radiation, creating a spatially uniform power distribution on the surfaces of samples (~1000 $W \cdot m^{-2}$) (Fig. S16, ESI†). Testing samples were placed on an insulation polystyrene foam substrate which reduces the influence of thermal conduction and thermal radiation from the bottom. Also, a polyethylene film was covered above the setup. A multi-channel thermometer (JINKO, JK804) connected with three K-type thermocouples was used to record the temperatures of the porous P(VDF-HFP) film, SRCP film, and the ambient air, respectively.

Section 1.4.2 Outdoor thermal measurements

Several setups were adopted to measure the outdoor cooling ability of the SRCP samples. The first setup mainly consists of two grooves of 8 cm × 8 cm × 2 cm on a large foam box of 45 cm × 30 cm × 28 cm. The grooves were covered by a porous P(VDF-HFP) film, and a SRCP film respectively. The entire foam box was wrapped with aluminum foil paper for shielding radiation from surrounding buildings. To shield the influence of thermal convection, a polyethylene film was covered above the setup. The foam box was placed 0.4 meters high away from the ground. Two thermocouples were placed inside the grooves to record the cooling temperature. One thermocouple was placed outside to record the PE shield air temperature. A datalogging solar power meter (TES-132) was used to simultaneously measure the hemispherical I_{solar}. (Fig. 3c, d). The second setup was adopted as reported before[1]. Simply, a piece of porous P(VDF-HFP)/PDMS film was covered on a polystyrene foam box. The box was placed in a paper box wrapped with aluminum foil paper for shielding radiation from surrounding buildings. One thermocouple was placed inside the polystyrene foam box to record the cooling temperature. Another thermocouple was placed outside to record the ambient temperature. (See ESI Fig. S21 a, b†). The third setup consisted mainly of three grooves of 10 cm × 10 cm × 2 cm on a large foam board. The three grooves were covered by a commercial thermal reflective material, a transparent polyethylene film, and a SRCP film respectively (See ESI Fig. S21 e, f†). The temperatures inside the grooves as well as the ambient temperature were tracked over time. The foam board was placed 0.4 meters high away from the ground. The measurement was conducted under direct sunlight on the rooftop of building or on the sports field's lawn. The experimental site was located at Xi'an, Shaanxi (34° 38' 64" N, 108° 9' 80" E, 600 m altitude).

In order to test the performance of the SRCP film as a thermal armor, we conducted a series of outdoor experiments. Firstly, under strong sunlight (the ambient temperature of the roof top ~ 40°C), two model cars were placed atop a foam box, with one being covered by the SRCP film with a diameter of 100 mm while another being exposed to the sun. A thermocouple was placed inside each car to measure the temperature and IR pictures were taken to examine the cooling performance.

Section 2. Supplementary Text

Section 2.1 Calculation of sun reflectance, thermal emittance of SRCP film

To achieve daytime radiative cooling, the SRCP film surface should have a high hemispherical sun reflectance ($\bar{R}_{sun}$) to minimize absorbing heat from sun and a high hemispherical thermal infrared emittance ($\bar{E}_{TIR}$) to maximize radiative heat loss to the sky. Briefly,

$$\bar{R}_{sun} = \frac{\int_{300nm}^{2500nm} I_{sun}(\lambda)R_{sun}(\lambda)d\lambda}{\int_{300nm}^{2500nm} I_{sun}(\lambda)d\lambda} \tag{E1}$$

where the 300-2500 nm represent the solar spectrum; λ is the wavelength; $R(\lambda)$ is the sample surface's reflectance spectra; $I_{sun}(\lambda)$ is the AM 1.5 solar spectral radiation defined by ISO standard 9845-1 (1992) [2].

$$\bar{E}_{TIR} = \frac{\int_{8\mu m}^{13\mu m} I_B(\lambda,T)(1-R_{TIR}(\lambda))d\lambda}{\int_{8\mu m}^{13\mu m} I_B(\lambda,T)d\lambda} \tag{E2}$$

$$I_B(\lambda,T)=\frac{2hc^2}{\lambda^5\left(e^{\frac{hc}{\lambda K_B T}}-1\right)} \tag{E3}$$

where the 8-13 μm bounds represent the thermal infrared transparent window, $R_{TIR}(\lambda)$ is the SRCP film surface's reflectance in the thermal infrared spectrum. The emissivity spectrum was obtained by measuring the reflectivity (R_{TIR}), which was calculated using Equ. E2, in which transmittance can be ignored (It follows Kirchhoff's law of thermal radiation states). $I_B(\lambda,T)$ is the blackbody radiation at temperature T according to Planck's law (E3), where c is the speed of light, λ is the wavelength, h is Planck's constant, and k_B is the Boltzmann constant.

Section 3. Figs S1 to 26

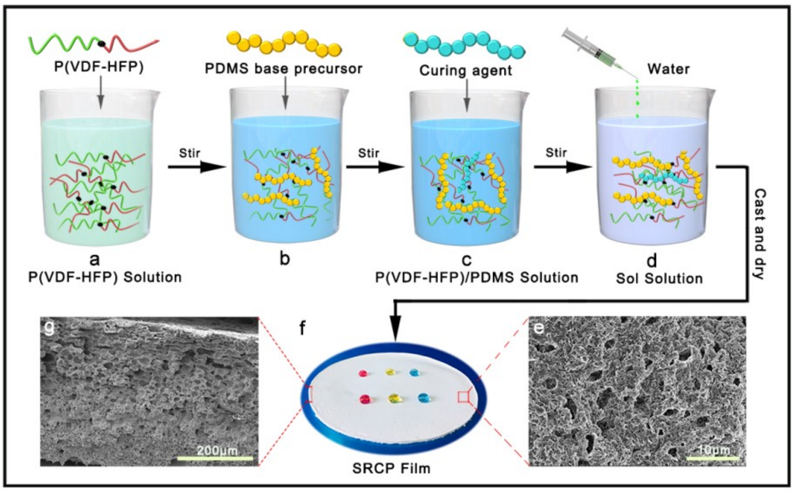

Fig. S1 Schematic of the fabrication process of SRCP film. a-d, The detailed fabrication procedures. **e,** SEM image of the as-fabricated film surface. **f,** Optical image of the SRCP film with water droplets deposited on the surface. **g,** Cross-sectional SEM image of the as-fabricated film.

Fig. S2 Digital photographs of other scalable SRCP films have surface roughness synergistic with internal hierarchical porous structure. a, SRCP PVDF/PDMS film, **b,** SRCP SEBS/SiO_2 film and **c,** SRCP PDMS/SiO_2 film.

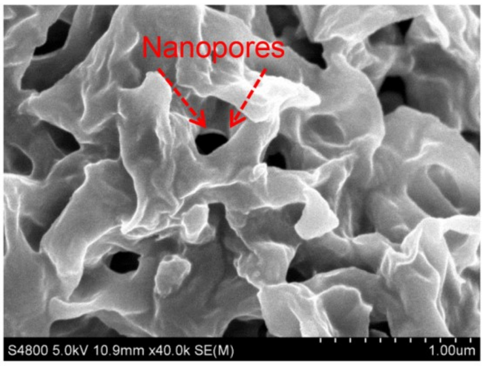

Fig. S3 SEM of the SRCP film showing nanostructures and nanopores.

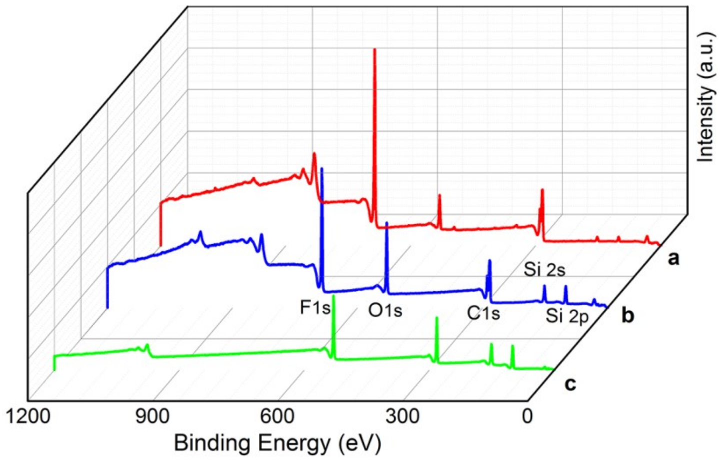

Fig. S4 XPS spectra of porous P(VDF-HFP), SRCP, PDMS films. a, Porous P(VDF-HFP) film. **b,** SRCP film. **c,** PDMS film.

Supplementary Table 1 The surface chemical composition of the films determined using XPS analysis. **a,** Porous P(VDF-HFP) film. **b,** SRCP film. **c,** PDMS film.

Samples	Element content (wt.%)			
	C	O	F	Si
a	62.29	8.40	29.31	--
b	49.91	14.87	16.25	18.97
c	23.04	44.35	--	32.61

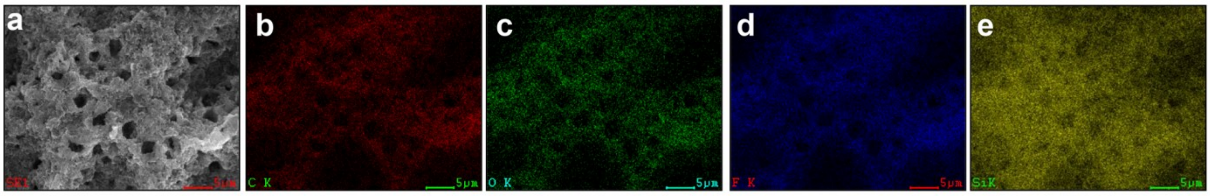

Fig. S5 EDS mapping images of the SRCP films. a, SEM images**. b,** Element C. **c,** Element O. **d,** Element F. **e,** Element Si.

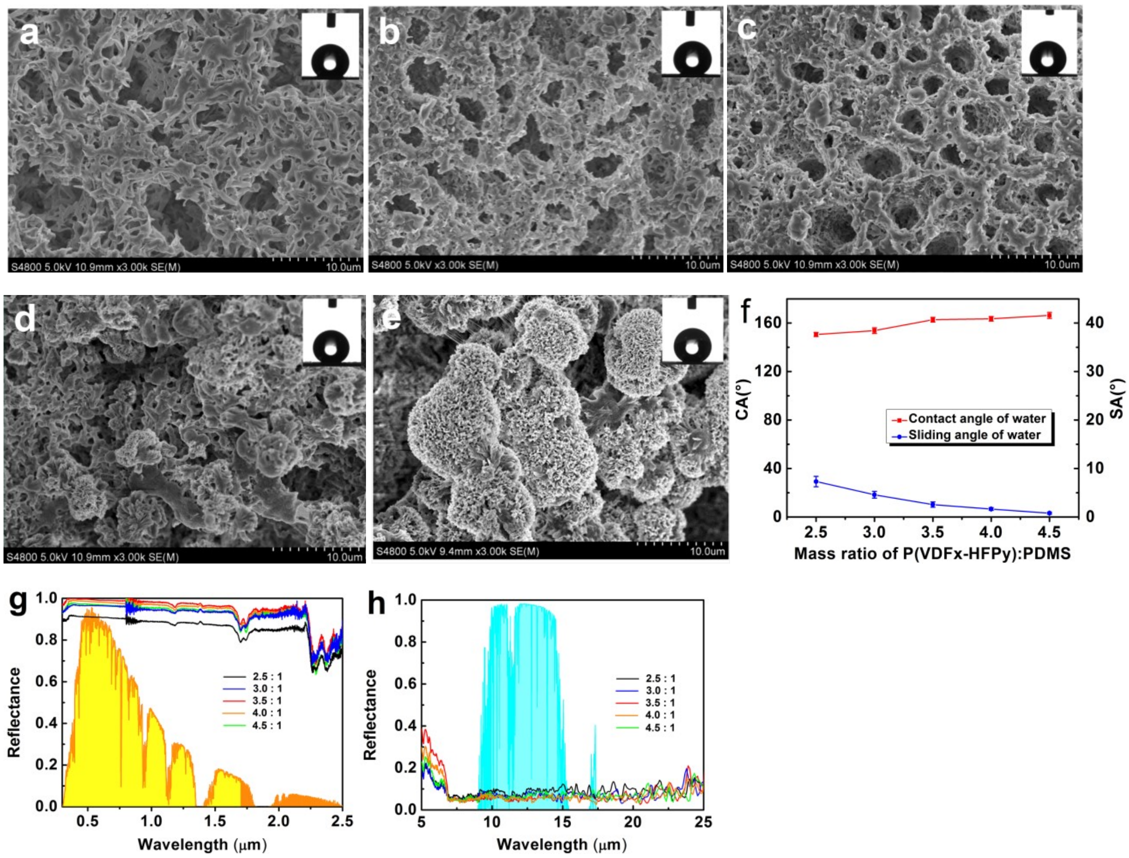

Fig. S6 SEM images of the SRCP films with different mass ratio of P(VDF-HFP) relative to PDMS. a, 2.5:1.0. **b,** 3.0:1.0. **c,** 3.5:1.0. **d,** 4.0:1.0. **e,** 4.5:1.0. The insets are snapshot of water droplet for measuring CA. **f,** Effect of the mass ratio of P(VDF-HFP) to PDMS on CA and SA of the SRCP film. **g , h,** Reflectance spectra of the fabricated SRCP film with rations of mP(VDF-HFP) : mPDMS from 2.5:1 to 4.5:1 in normalized AM 1.5 solar spectrum (yellow shaded area) and atmospheric transparency window (light blue shaded area).

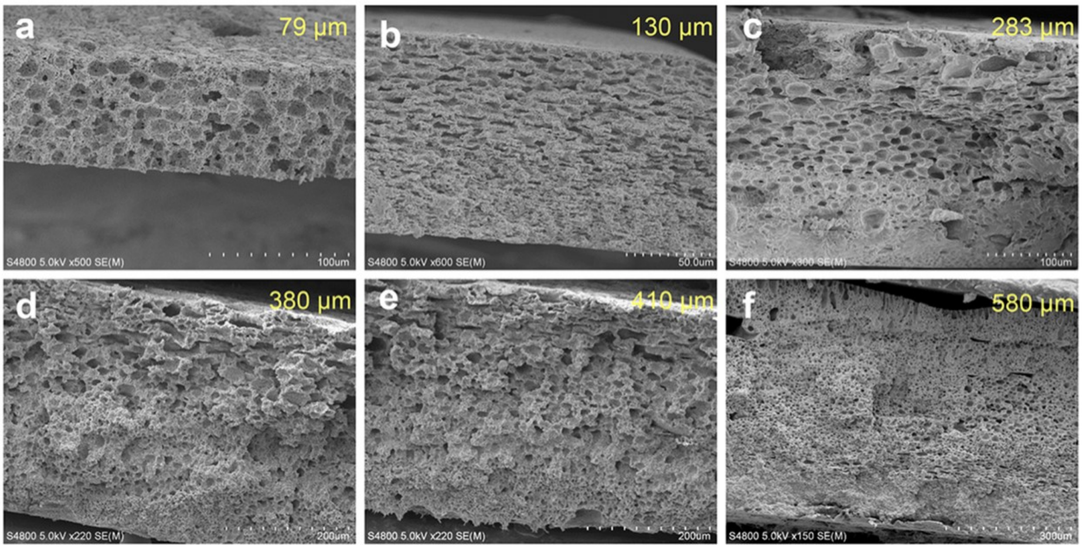

Fig. S7 Cross-sectional SEM images of SRCP films with different thickness. a, 79 μm. **b,** 130 μm. **c,** 283 μm. **d,** 380 μm. **e,** 410 μm. **f,** 580 μm.

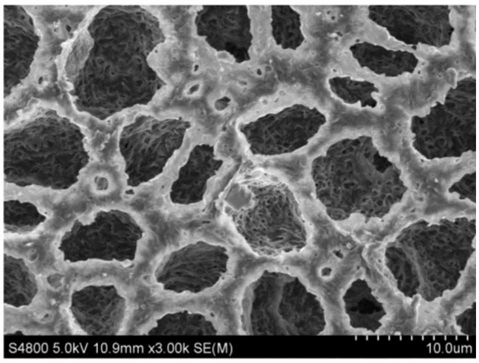

Fig. S8 SEM image of the porous P(VDF-HFP) film that mainly consists of micropores on the surface.

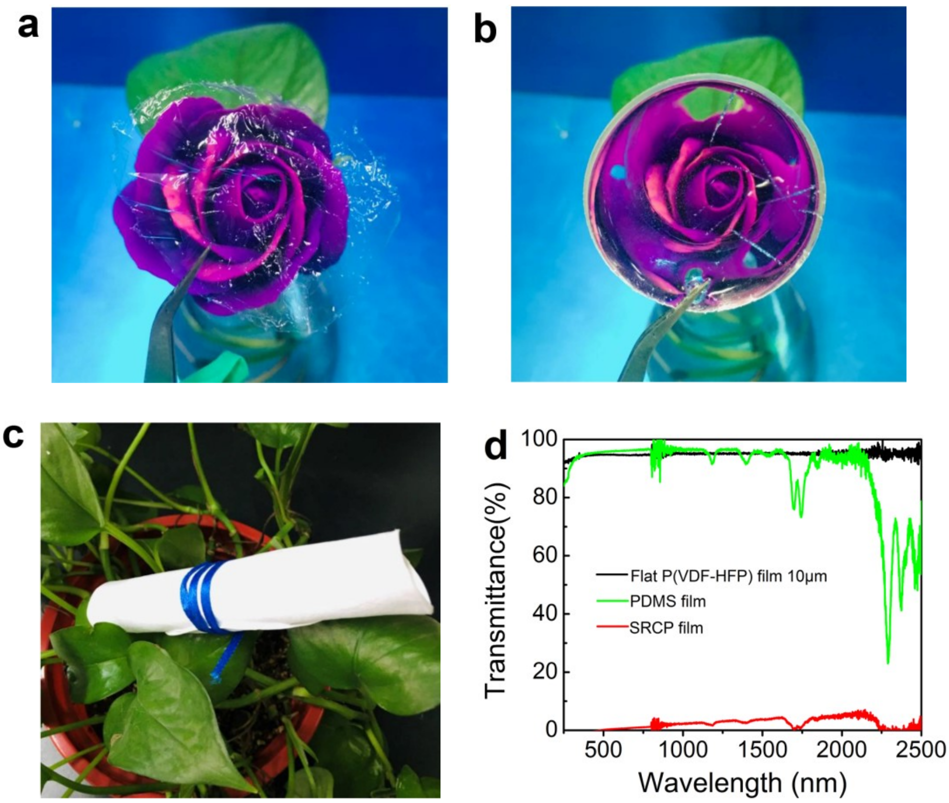

Fig. S9 Digital photographs of different films and their transmittance. a, Flat P(VDF-HFP) film (10 μm). **b,** Transparent PDMS films. **c,** Free-standing SRCP film rolled with high flexibility which can be easily curled. **d,** Transmittance of the flat P(VDF-HFP) film (black curve), transparent PDMS film (green curve) and SRCP film (red curve).

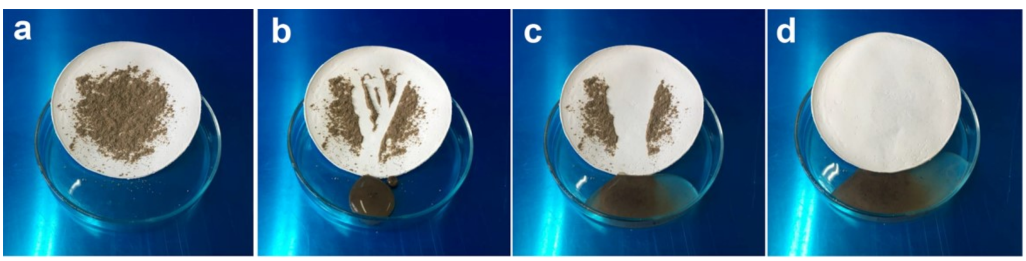

Fig. S10 Self-cleaning property. a-d, Photographs of self-cleaning test of the SRCP film with dust removed by water.

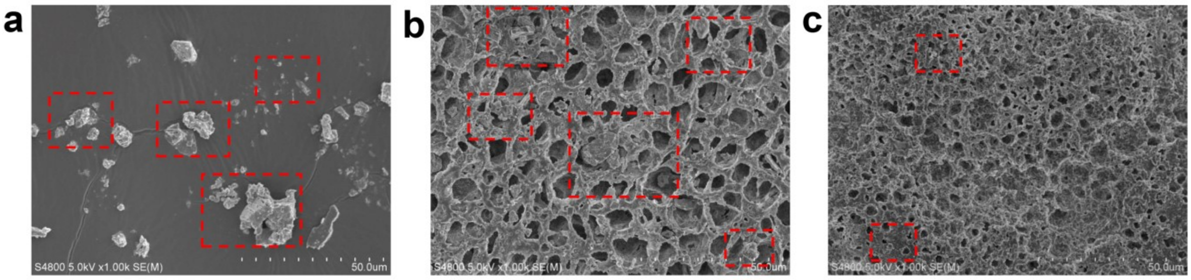

Fig. S11 SEM imgaes of the films after outdoor exposure for one month. a, b, Flat P(VDF-HFP) and porous P(VDF-HFP) film shoeing particles of dust attached. **c,** SRCP film showing no contamination occurred.

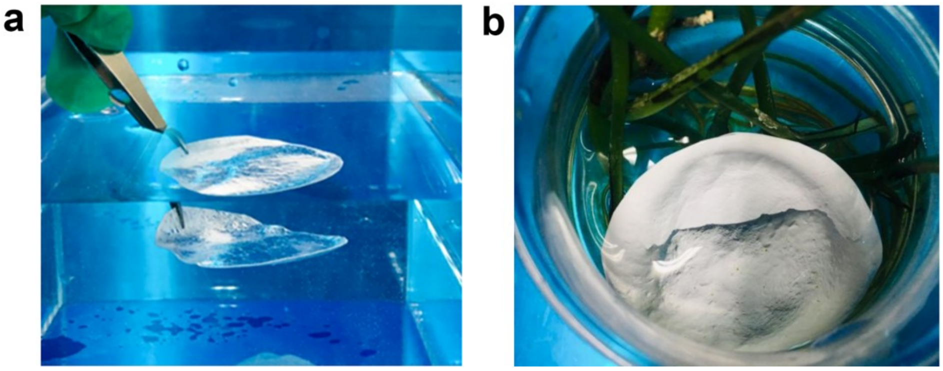

Fig. S12 Superhydrophobic property of SRCP film. a, Digital photograph of the silver mirror phenomenon of the SRCP film under water. **b,** Digital photograph of the silver mirror phenomenon of the SRCP film after immersion in water for 14 days (The air interface and the water interface totally reflect the light to see the silver color like a mirror, because the "air cushion structure" produced by the superhydrophobic micro-nano structure makes the film form a solid, gas, and liquid three-phase interface under water).

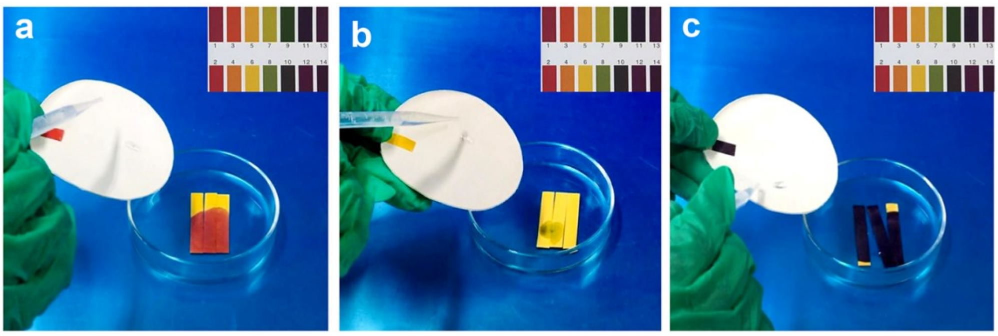

Fig. S13 Resistance of the SRCP film to acid, water and salt solutions. a-c, Photographs of the solution (acid, water, alkali) rolling off the SRCP film.

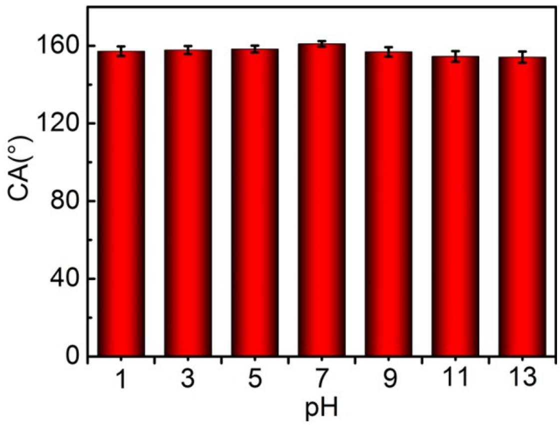

Fig. S14 Variation of CA of SRCP films after soaking in solutions of different pH for one month.

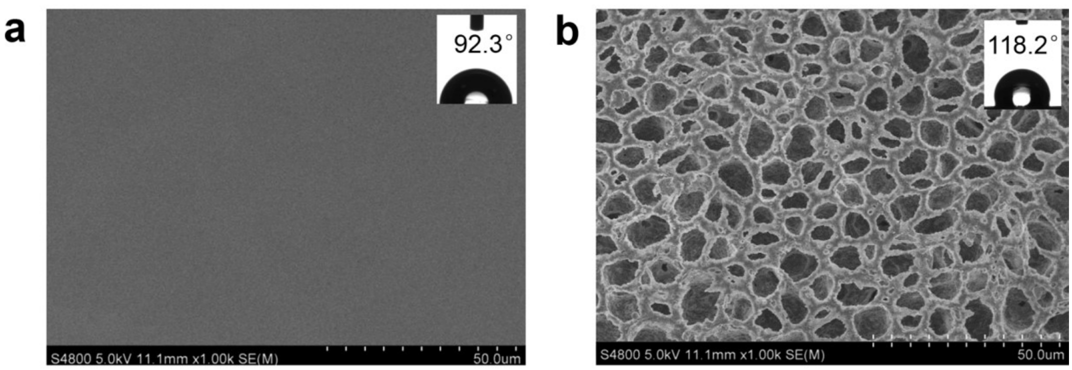

Fig. S15 Wetting of the flat P(VDF-HFP) film and porous P(VDF-HFP) film. a, SEM of flat P(VDF-HFP) with inset of the CA of 92.3 ± 0.2°. **b,** SEM of porous P(VDF-HFP) film with inset of the CA of 118.2 ± 0.4°.

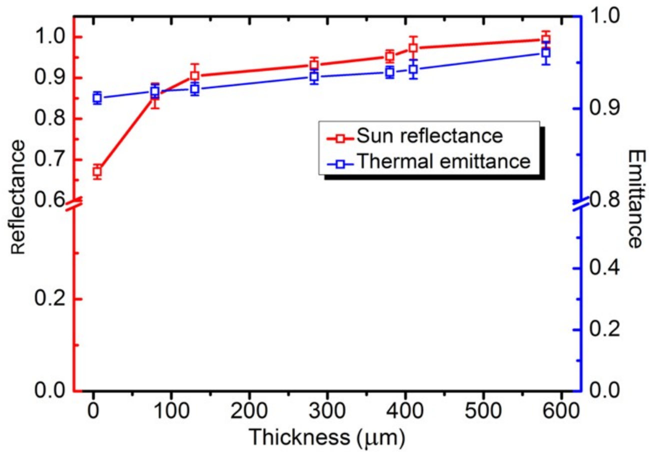

Fig. S16 Sun reflectance and thermal emittance of the SRCP films with different thicknesses.

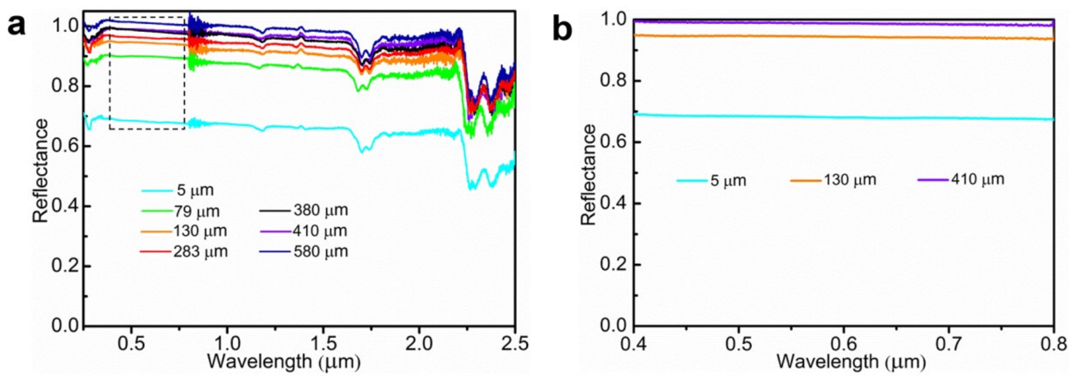

Fig. S17 Solar reflectance curves of SRCP films with different thicknesses. a, Effect of the SRCP film thickness on the solar reflection (The thickness of the samples was 5 μm, 79 μm, 130 μm, 283 μm, 380 μm, 410 μm, and 580 μm, respectively). **b,** Integrated reflectance spectrum for the freestanding SRCP films of 130 μm, 410 μm and ultrathin (5 μm thick) porous films at visible wavelengths, excluding specular reflections. The ultrathin 5 μm thick film was obtained by casting on a glass substrate (See ESI Fig. S18†).

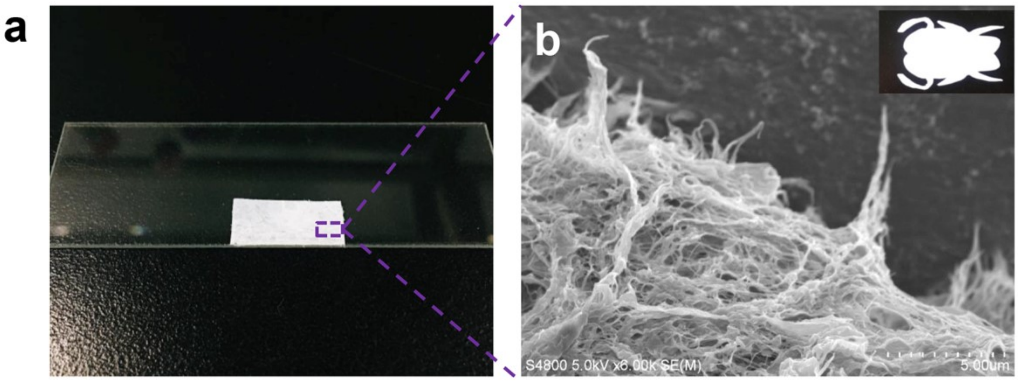

Fig. S18 The photo and SEM of a 5 μm thick SRCP film. a, The film is 5 μm thick obtained by spinning on a transparent glass substrate. **b,** Cross-sectional SEM image of the SRCP film, revealing the random networks that cause the bright white coloration (inset) by multiple light scattering.

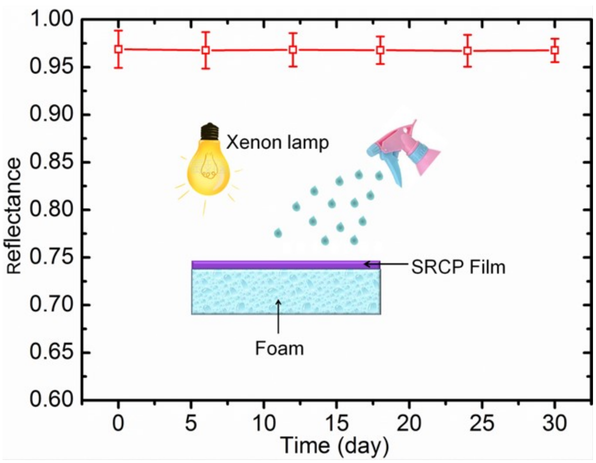

Fig. S19 Change of reflectance of the SRCP film after Xenon lamp irradiation with water mist sprayed to alternately accelerate aging of the film for one month.

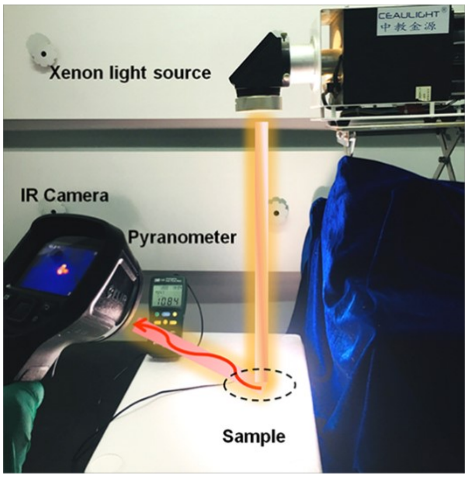

Fig. S20 Photo of the thermodynamic experimental simulation device using a Xenon lamp (Zhongjiao Jinyuan HXF300) with a high power which matches well with the solar spectrum to simulate solar radiation (The spectral range is 300-2500nm), creating a spatially uniform power distribution at the sample's surface (~1000 $W \cdot m^{-2}$).

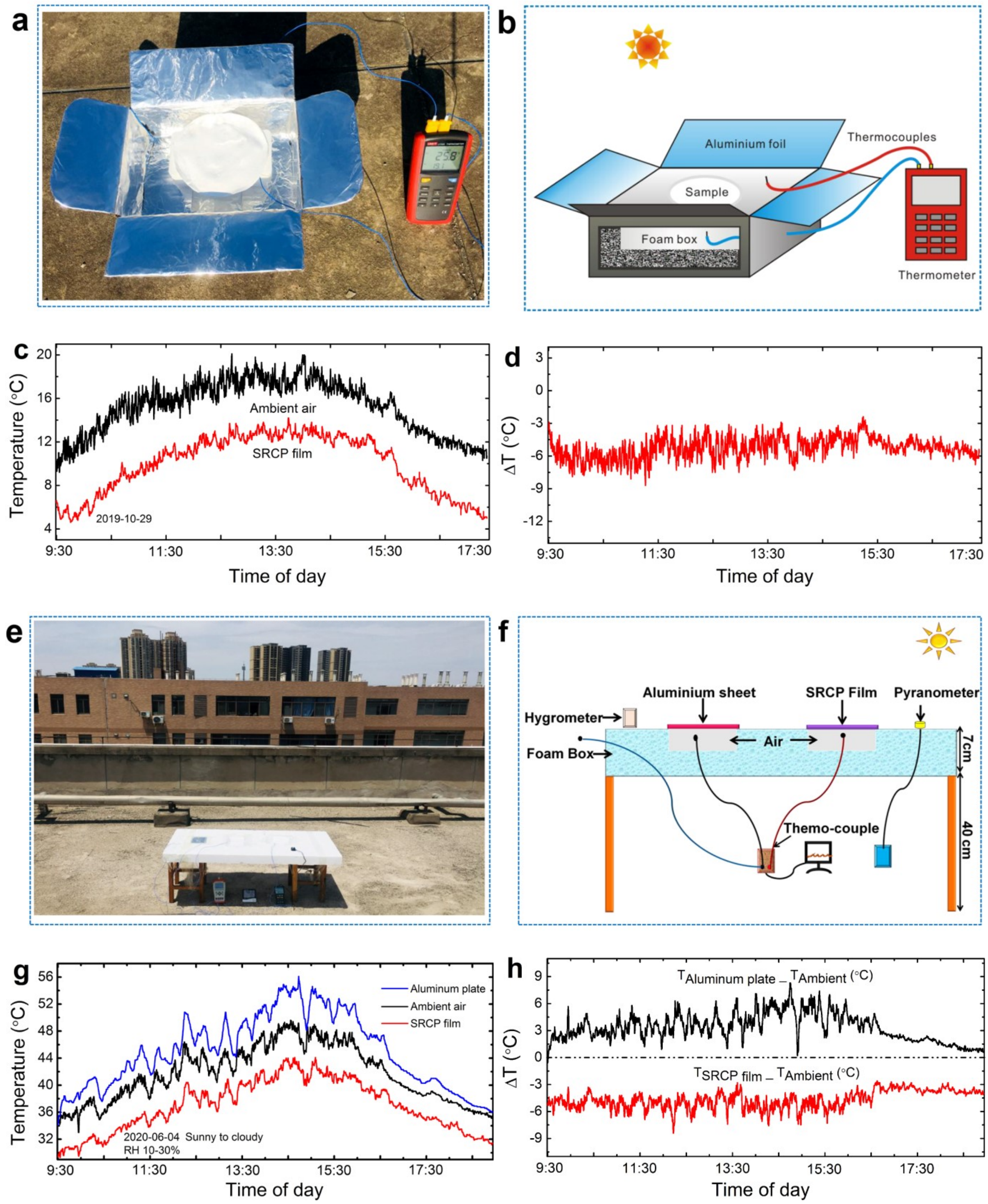

Fig. S21 Daytime radiative cooling performance of the SRCP film. a, Foam box covered by a 150-mm-diameter SRCP film on a clear autumn day. **b,** Illustration of the setup of a. **c,** Real-time temperature of ambient air (black curve) and the inside of the box (red curve) for a. **d,** Temperature difference ($T_{SRCP\ film}$ - $T_{ambient}$) for c. **e,** Photo of the setup on the roof of the building complex on a hot summer day (RH 10-30%). **f,** Illustration of the setup of e. **g,** Real-time temperatures of ambient air (black curve) and the inside of the groove covered by SRCP film (red curve) and aluminum plate (blue curve). **h,** Temperature difference of SRCP film and aluminum plate compared to the ambient air for g.

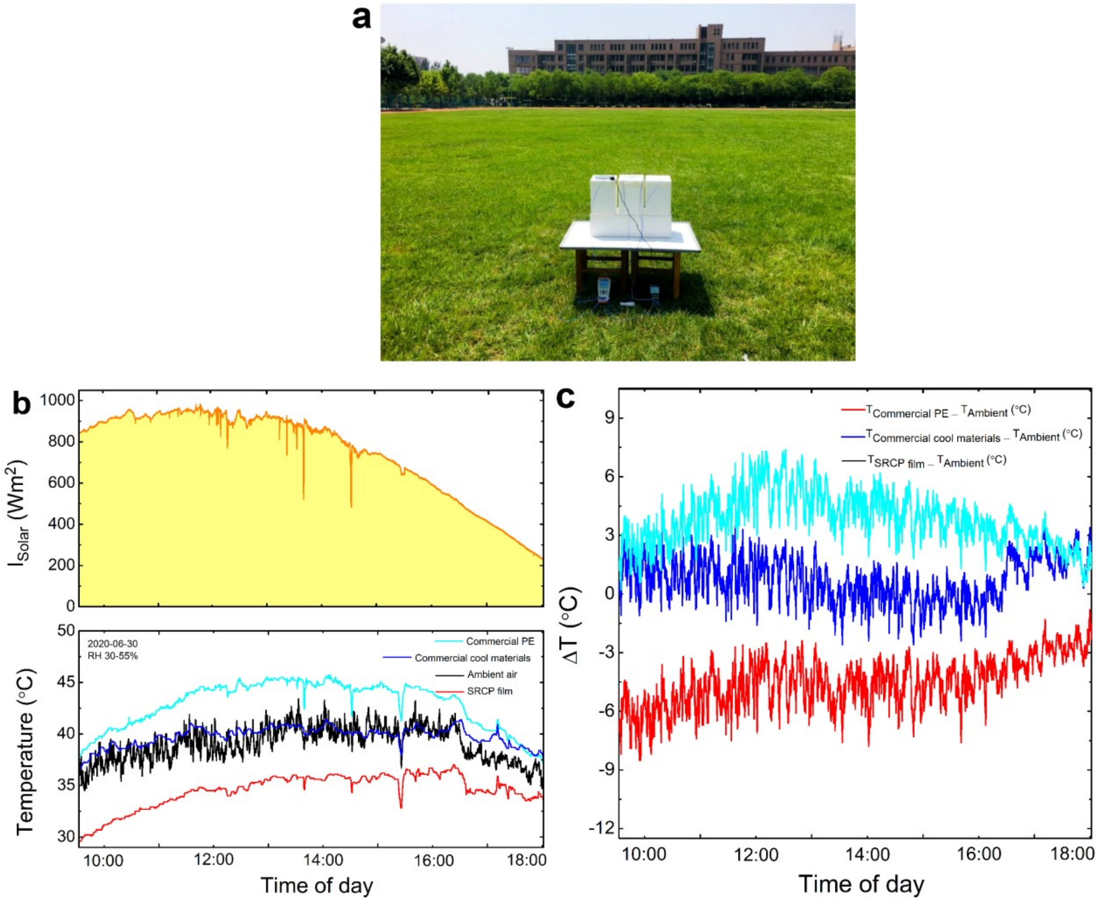

Fig. S22 Daytime radiative cooling performance of the SRCP film in the lawn center of a sports field (exposed to the ambient air without any radiation and convection shielding). **a,** Photo of the setup of 14 cm × 12 cm × 16 cm foam boxes on the lawn. **b,** Solar intensity (top) and real-time temperatures of foam boxes covered by commercial PE, commercial cool material and SRCP film and of ambient air. **c,** Temperature difference of commercial PE, commercial cool material and SRCP film covered boxes compared to the ambient air for b.

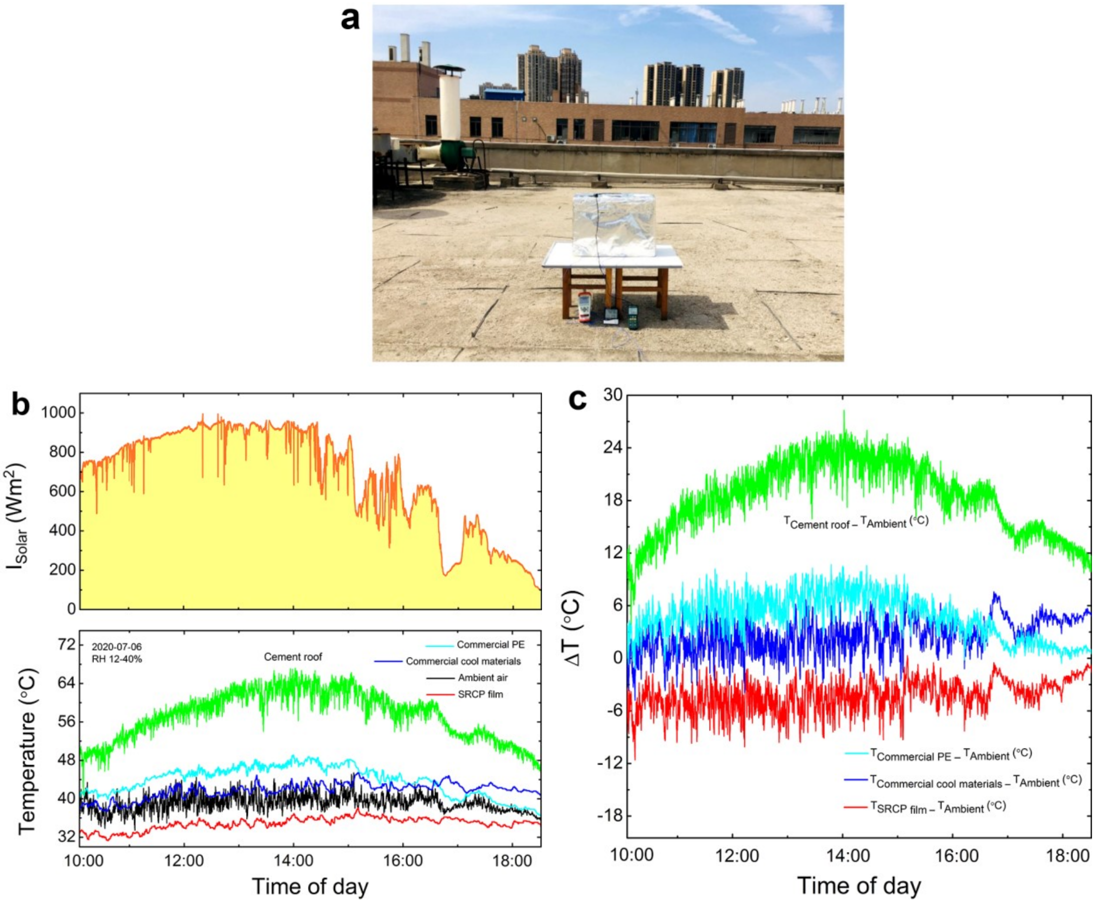

Fig. S23 Daytime radiative cooling performance of the SRCP film in the building roof (exposed to the ambient air without any convection shielding). a, Photo of the setup of 14 cm × 12 cm × 16 cm foam boxes wrapped by aluminum foil on the building roof. **b,** Solar intensity (top) and real-time temperatures of foam boxes covered by commercial PE, commercial cool material and SRCP film and of ambient air. **c,** Temperature difference of commercial PE, commercial cool material and SRCP film covered foam boxes compared to the ambient air for b.

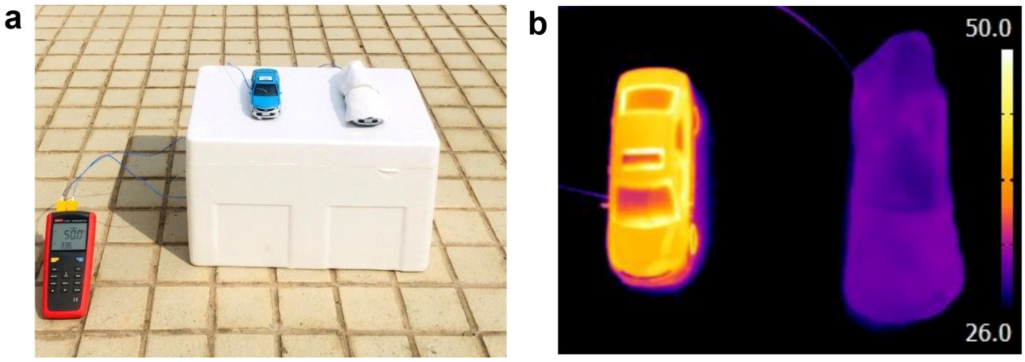

Fig. S24 a, Digital pictures showing the tested temperatures of two identical car models with and without SRCP film. **b,** IR picture of the cars in a.

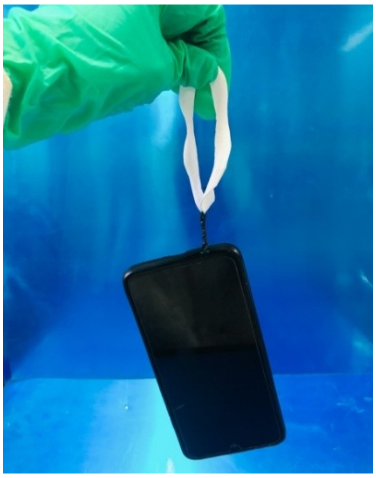

Fig. S25 Digital photo of a string cut from a 130 μm thick SRCP film withstanding the weight of a 150 g phone.

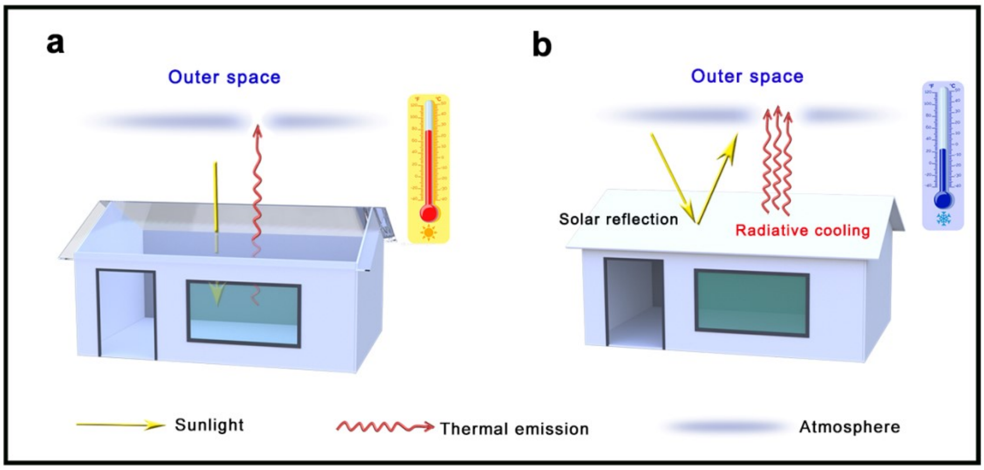

Fig. S26 Conventional roofing materials and SRCP film as roofing materials. a, Conventional roof materials absorb heat from the sun, but dissipate less heat as emission. **b,**

When being used as a roofing material, the SRCP film exhibits high solar reflectance and high infrared emissivity.

Section 4. Supplementary Tables.

Table S1. Comparison of the performances of our work with some typical reports.

Radiative cooler	Testing time	Reflectance/ emittance	Temperature drop (°C)	Contact/ sliding Angle (°)	Testing setup	Journals
Ref.1 (inorganic structure)	13:00-14:00	0.97/-	4.9 °C	—	Shielded by PE*	Nature
Ref.2 (inorganic structure)	15:00	0.97/0.75	8 °C(Max)	—	Shielded by PE*	Sol.Energy Mater .Sol.Cells
Ref.3 (porous metallic)	Whole day	0.86/0.96	6.1 °C(Max)	—	Shielded by PE*	Nano energy
Ref.4 (porous metallic)	Night	-/0.95	2.6 °C	—	Shielded by PE*	Sol.Energy Mater .Sol.Cells
Ref.5 (metal-polymer)	—	0.8/0.9	6 °C(Max)	—	Shielded by PE*	Nat. Commun.
Ref.6 (metal-polymer)	11:00-15:00	-/-	11 °C	—	Shielded by PE*	Nat. Sustain.
Ref.7 (polymer composites)	11:00-14:00	-/0.93	—	—	Shielded by PE*	Science
Ref.8 (polymer composites)	11:30-15:30	0.898/0.96	6 °C	—	Exposed to the environment	Adv. Mater.
Ref.9 (polymer composites)	12:00-14:30	0.95/0.96	5.1 °C	CA ~138°	Shielded by PE*	PANS.
Ref.10 (polymer composites)	11:00-13:00	0.95/0.96	8.1 °C(Max)	CA =125.3°	Exposed to the environment	Nano energy
Ref.11 (porous wood)	11:00-14:00	0.96/-	4 °C	CA ~150°	Shielded by PE*	Science
Ref.12 (porous polymer)	13:00-14:00	0.96/0.97	6 °C	CA =110°	Exposed to the environment	Science
Ref.13 (porous polymer)	12:00-14:00	0.95/0.98	8.9° C	CA ~156°	Shielded by PE*	Nat. Commun
Ref.14 (porous polymer)	12:00-12:30	0.93/0.94	5 °C	—	Shielded by PE*	Adv. Mater.
Ref.15 (porous polymer)	11:00-13:00	0.96/0.97	6 °C(Max)	—	—	Adv. Funct. Mater.
Ref.16 (porous polymer)	12:30-15:30	0.963/0.78	5 °C	—	Shielded by PE*	Nature Nanotech.
Ref.17 (nanocomposite)	12:00-15:00	0.88/0.92	3.6 °C	CA =159± 2.5° SA = 6.8°	Shielded by PE*	ACS Appl. Mater. Interfaces
Ref.18 (cotton fabric)	—	0.90/0.92	—	CA =151.9± 0.9° SA = 1.3 ± 0.3°	Shielded by PE*	Chem. Eng.J.
This work	**12:00-14:00**	**0.965/0.943**	**13.8 °C**	**CA =162.3 ± 1.0° SA = 2.0 ± 0.6°**	**Shielded by PE***	

Shielded by PE* to minimize the influence of thermal convection from surroundings.
— means no data were shown in the papers.

Section 5. Supplementary Videos

Video S1: Comparison of anti-contamination and self-cleaning properties of SRCP film and conventional PDRC materials.

The SRCP film kept its original white color when being poured by muddy water, whereas the porous P(VDF-HFP) film was easily stained. The video was replayed at the real time.

Video S2: Durability of the SRCP film in acid, alkali and salt environments.

The SRCP film surface remains a robust superhydrophobic property against acidic, alkali and salt liquids. The video was replayed at the real time.

Video S3: Flexibility and heat dissipation performance of the SRCP film.

The SRCP film is repeatedly rubbed and still maintains the original shape. Infrared camera measurement shows the quick heat dissipation. The video was replayed at ×3.5 times speed.

Section 6. References

1 A. P. Raman, M. A. Anoma, L. Zhu, E. Rephaeli, S. Fan, *Nature,* 2014, **515**, 540.

2 H. Ma, K. Yao, S. Dou, M. Xiao, M. Dai, L. Wang, H. Zhao, J. Zhao, Y. Li, Y. Zhan, *Sol. Energy Mater. Sol. Cells.,* 2020, **212**, 110584.

3 D. Lee, M. Go, S. Son, M. Kim, T. Badloe, H. Lee, J.K. Kim, J. Rho, *Nano Energy,* 2021,**79**, 105426.

4 Y. Fu, J. Yang, Y. Su, W. Du, Y. Ma, *Sol. Energy Mater. Sol. Cells.,* 2019, **191**, 50.

5 B. Bhatia, A. Leroy, Y. C. Shen, L. Zhao, M. Gianello, D. H. Li, T. Gu, J. J. Hu, M. Soljacic, E. N. Wang, *Nat. Commun.,* 2018, **9**, 5001.

6 L. Zhou, H. Song, J. Liang, M. Singer, M. Zhou, E. Stegenburgs, N. Zhang, C. Xu, T. Ng, Z. Yu, B. Ooi, Q. Gan, *Nat. Sustain.,* 2019, **2**, 718.

7 Y. Zhai, Y. G. Ma, S. N. David, D. L. Zhao, R. N. Lou, G. Tan, R. G. Yang, X. B. Yin, *Science,* 2017, **355**, 1062.

8 X. Xue, M. Qiu, Y. Li, Q. M. Zhang, S. Li, Z. Yang, C. Feng, W. Zhang, J.-G. Dai, D. Lei, W. Jin, L. Xu, T. Zhang, J. Qin, H. Wang, S. Fan, *Adv. Mater.,* 2020, **32**, 1906751.

9 H. Zhang, KCS. Ly, X. Liu, Z. Chen, T. Fan, *Proc. Natl. Acad. Sci. USA.,* 2020, **117**, 14657.

10 Zcab, D, Han, H, Fwb, C, Yy, D, Xsa, B, & Hla, *Nano Energy,* 2021, **89**, 106377.

11 T. Li, Y. Zhai, S. He, W. Gan, Z. Wei, M. Heidarinejad, D. Dalgo, R. Mi, X. Zhao, J. Song, J. Dai, C. Chen, A. Aili, A. Vellore, A. Martini, R. Yang, J. Srebric, X. Yin, L. Hu, *Science,* 2019, **364**, 760.

12 J. Mandal, Y. Fu, A. C. Overvig, M. Jia, K. Sun, N. N. Shi, H. Zhou, X. Xiao, N. Yu, Y. Yang, *Science,* 2018, **362**, 315.

13 T. Wang, Y. Wu, L. Shi, X. Hu, M. Chen, L. Wu, *Nat. Commun*., 2021, **12**, 365.

14 H. Zhao, Q. Sun, J. Zhou, X. Deng, J. Cui, *Adv. Mater*., 2020, **32**, 2000870.

15 X. Wang, X. H. Liu, Z. Y. Li, H. W. Zhang, Z. W. Yang, H. Zhou, T. X. Fan, *Adv. Funct. Mater*., 2019, **30**, 1907562.

16 D. Li, X. Liu, W. Li, Z. Lin, B. Zhu, Z. Li, J. Li, B. Li, S. Fan, J. Xie, J. Zhu, *Nat. Nanotechnol*., 2021, **16**, 153.

17 S. Zhong, L. Yi, J. Zhang, T. Xu, L. Xu, X. Zhang, T. Zuo and Y. Cai, *Chem. Eng. J.*, 2020, **407**, 127104.

18 S. Wang, Y. Wang, Y. Zou, G. Chen, J. Ouyang, D. Jia and Y. Zhou, *ACS Appl. Mater. Interfaces*., 2021, **18**, 13.